# Sub-nA spatially resolved conductivity profiling of surface and interface defects in ceria films

# Sub-nA spatially resolved conductivity profiling of surface and interface defects in ceria films

Tim Farrow, Nan Yang, Sandra Doria, Alex Belianinov, Stephen Jesse, Thomas M. Arruda, Giuseppe Balestrino, Sergei V. Kalinin, and Amit Kumar

Citation: APL Materials **3**, 036106 (2015); doi: 10.1063/1.4914943
View online: http://dx.doi.org/10.1063/1.4914943
View Table of Contents: http://scitation.aip.org/content/aip/journal/aplmater/3/3?ver=pdfcov
Published by the AIP Publishing

# Sub-nA spatially resolved conductivity profiling of surface and interface defects in ceria films

Tim Farrow,[1] Nan Yang,[2] Sandra Doria,[3] Alex Belianinov,[4] Stephen Jesse,[4] Thomas M. Arruda,[5] Giuseppe Balestrino,[3] Sergei V. Kalinin,[4] and Amit Kumar[1,a]

[1]*Centre for Nanostructured Media, School of Mathematics and Physics, Queen's University Belfast, Belfast BT7 1NN, United Kingdom*
[2]*CNR-SPIN and Engineering Faculty, Università degli studi Niccolò Cusano, Rome I-00166, Italy*
[3]*CNR-SPIN and DICCI Dipartiment, Università di Roma Tor Vergata, Via del Politecnico 1, I-00133 Rome, Italy*
[4]*Center for Nanophase Materials Sciences, Oak Ridge National Laboratory, Oak Ridge, Tennessee 37831, USA*
[5]*Chemistry Department, Salve Regina University, Newport, Rhode Island 02840, USA*

(Received 12 January 2015; accepted 3 March 2015; published online 17 March 2015)

Spatial variability of conductivity in ceria is explored using scanning probe microscopy with galvanostatic control. Ionically blocking electrodes are used to probe the conductivity under opposite polarities to reveal possible differences in the defect structure across a thin film of $CeO_2$. Data suggest the existence of a large spatial inhomogeneity that could give rise to constant phase elements during standard electrochemical characterization, potentially affecting the overall conductivity of films on the macroscale. The approach discussed here can also be utilized for other mixed ionic electronic conductor systems including memristors and electroresistors, as well as physical systems such as ferroelectric tunneling barriers.  [http://dx.doi.org/10.1063/1.4914943]

Coupling between electronic and ionic transport in solid oxides underpins an immense range of energy storage and conversion technologies. Such phenomena are further employed in macroscopic and nanoscale chemical sensors,[1–3] enabling the detection of a broad range of gaseous and liquid species and can be further utilized in electrochemical transducers.[4] Recently, a broad range of potential applications for ionic and mixed ionic electronic conductors (MIECs)[5,6] has emerged in information technologies for electroresistive memories and neuromorphic electronic devices.

Cerium oxide ($CeO_2$) is one of the most versatile and well-studied materials for solid-state electrochemical applications such as fuel cells[7] and electrolyzers.[8,9] These applications are based on the unique redox chemistry of pure and doped ceria. $CeO_2$ is a MIEC in which conductivity depends largely on deviations from stoichiometry due to impurities, oxygen vacancies, and oxygen activity in the ambient atmosphere with both ionic and electronic conductivities linked strongly to ambient temperature.[10,11] Ceria also exhibits high electronic conductivity at low partial pressures of oxygen due to the formation of small polarons hopping between the $Ce^{3+}$ and $Ce^{4+}$ valence states of cerium.[12] Ionic conductivity has been attributed to oxygen vacancies which arise from the high propensity of cerium oxides to reduce whilst retaining fluorite structure, depending on the ambient temperature and abundance of oxygen available. The conductivity of ceria can further be tailored by nanostructuring, e.g., nanocrystalline ceria is reported to have remarkable enhancement in electronic conductivity.[13] Similar to other MIEC materials, defects and interface layers can significantly

[a]Email: a.kumar@qub.ac.uk

 

affect the transport of oxygen vacancies and electrons in the material, thus directly affecting both its conductivity and overall functionality for integrated devices.

Classical electrochemical strategies for probing direct current (dc) transport, based on the use of polarizable/blocking electrodes[14,15] or impedance measurements on macroscopic systems, allow the decoupling of electronic and ionic transport as well as interface and bulk contributions. However, the *lateral* homogeneity of properties and even identification of specific elements remain a challenge. Furthermore, the limits on current and impedance detection typically limit these studies to micron-scale and larger systems, precluding information on the effects of local inhomogeneities from being obtained.

Here, we demonstrate that high-resolution current-voltage (I-V) mapping in scanning probe microscopy (SPM) can be used to visualize the spatial variation of conductance in ceria on the nanometer scale. The high electrochemical activity of this material and strong propensity towards irreversible electrochemical reactions necessitate galvanostatic control in I-V measurements, as is implemented here. We demonstrate that the spatial distribution of conductance is markedly different for cathodic and anodic voltage sweeps, suggesting that different processes are probed during the two procedures. Based on the qualitative analysis of the electronic-ionic transport processes, we interpret these inequalities as contrasting mobile defect contributions on the surface and in the bulk/bottom interface. This approach thus allows insight into surface and interface defects in similar MIEC thin films.

As a model system, we have chosen a 35 nm thick $CeO_2$ film grown epitaxially on a Nb doped $SrTiO_3$ (Nb:STO) substrate. The film was prepared using pulsed laser deposition and the X-ray diffraction studies revealed a single phase film oriented along the (100) direction. Preliminary current-voltage mapping for similar materials in ambient conditions by SPM has illustrated that the application of bias results in static surface deformation (irreversible expansion up to 10 nm for a 300 nm thick film) for positive bias application as low as 15 V. Deformation is also observed for cathodic processes when a negative bias is applied. The observed process is typically uncorrelated with current and is attributed to water and oxygen mediated reactions on the ceria surface.[16] In this work, we explore the spatially resolved transport behavior of this material in a glove box environment with <0.1 ppm of $O_2$ and 0.1 ppm of $H_2O$ (dry atmosphere), thus minimizing the possibility of water and oxygen mediated surface reactions.

In a dry atmosphere, static surface deformations are not observed for low currents. However, surface damage is observed once the current exceeds 1-2 nA range e.g. due to the reduction of ceria under positive applied bias and the formation of crystallographic shear phases.[17,18] This consideration severely affects the experimental strategy for I-V mapping. For example, the use of traditional approaches for conducting atomic force microscopy mapping, based on a voltage sweep up to a predefined voltage with simultaneous detection of current, is therefore impossible in this case. Namely, the I-V curves vary significantly on the sample surface and voltages that lead to irreversible surface deformation in some locations are insufficient to yield a measurable current in others, precluding high-resolution imaging. To obviate this problem, here we implement galvanostatic I-V measurements, in which the feedback loop interrupts the voltage sweep once the current achieves a predefined set point value (further referred to as the compliance limit).

As an illustration of conductance behavior in the ceria film under these conditions, Fig. 1 shows the I-V plots for 100 points on the film with a compliance limit of 1 nA in both 1(b) positive and 1(a) negative bias directions. An important point to note is the different shape of the curves for cathodic and anodic processes. In the anodic regime, the curves are super-exponential and at some point show a very rapid onset of current, suggesting a breakdown in the normal behavior possibly due to surface oxygen evolution or electroforming at such high current levels (e.g., compared to the behavior for other oxides).[19–21] The variability of the anodic I-V curves is also significantly larger than that of cathodic ones which instead show a more gradual exponential curvature, remaining stable to much greater biases which lack the same sudden breakdown behavior seen in some of the anodic curves.

To explore the *spatial variability* of conductance behavior in ceria thin films, we have performed ***dense*** I-V curve measurements in the galvanostatic regime. In these measurements, a bias sweep in positive or negative directions is applied to the tip (note that bipolar sweeps typically led

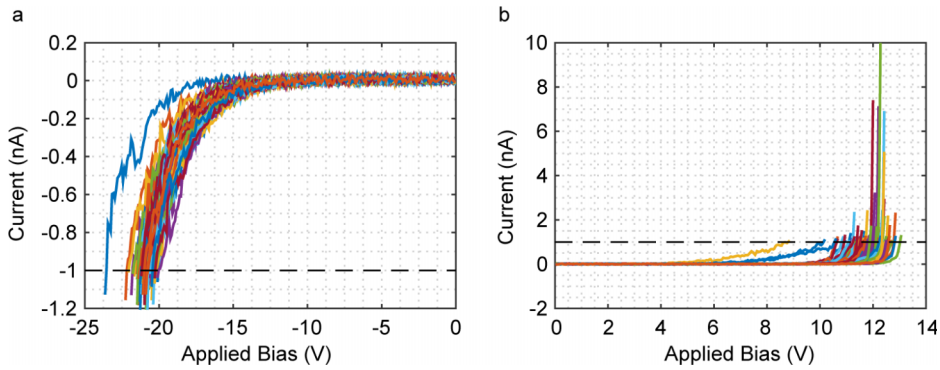


FIG. 1. (a) I-V plots for 100 points on the $CeO_2$ film grown on Nb:STO for negative bias with a compliance limit of −1 nA. (b) I-V plots for the same 100 points for positive bias with a compliance limit of 1 nA.

to rapid surface and tip degradation, necessitating sequential cathodic and anodic mapping). The sweep is applied until the current reaches the limiting current and is then terminated. The bias and current are recorded to yield the I-V curve at the selected location. This measurement was repeated across a dense spatial grid (60 × 60 points over 1 $\mu$m square) to obtain a dense map of I(x,y,V). Note that the number of voltage points recorded depends on location due to different compliance cutoffs. Here, the limiting current is kept very small (100 pA) to minimize irreversible electrochemical reactions and enable high-resolution cathodic and anodic mapping. It is also important to point out the result is quite repeatable even while measuring twice at a same point.

Topographic images taken before and after the cycling measurements with the 100 pA cutoff current are shown in Figs. 2(a) and 2(b), respectively. There is no detectable topographic change (within 100 pm) during these measurements, suggesting that the measurement reveals the intrinsic conductivity of the ceria film unaffected by (irreversible) decomposition and phase formation reactions or surface contamination dynamics.[22] Comparisons to the first 100 points measured with a higher compliance current can be made between Fig. 1 and the IV curves shown in Figs. 3(a) and 3(b). Here, the similarity in the curvature between the positive and negative bias sweeps can be seen although the positive bias measurements still show a greater variation in voltage cutoffs and some points can be noted as having some form of electrical breakdown. A 2D histogram showing joint probability distribution for positive and negative compliance voltages is shown in Fig. 3(c). Note the overall Gaussian shape and broader distribution for anodic compliance voltages, as well as the lack of correlation between positive and negative cutoff biases (the joint probability distribution is well approximated by product of individual probabilities), suggesting that the two are independent on most of the surface.

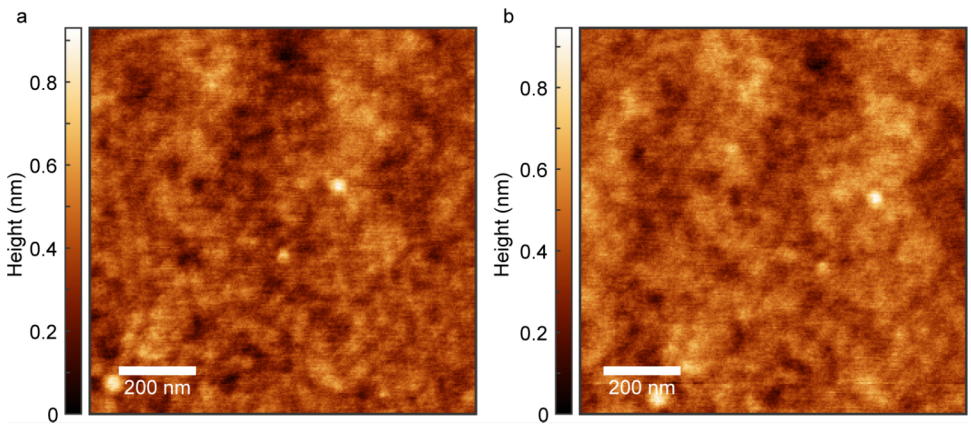


FIG. 2. Surface topography scans of 1 $\mu$m square ceria surface (a) before 100 pA compliance current mapping and (b) after.

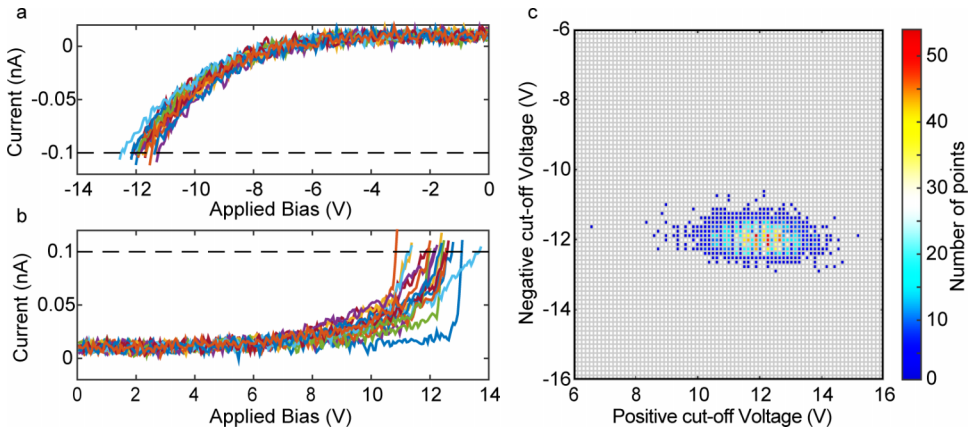


FIG. 3. (a) I-V plots for a selection of points (60×60 array) across 1 $\mu$m square $CeO_2$ surface of negative bias with a compliance limit of −100 pA and (b) positive bias over the same area. The relative confinement of negative compliance voltages with respect to positive compliance voltages is shown in (c) as a 2D histogram.

To interpret the spatial variability of the surface and to compare against topography, 2D plots of the bias corresponding to the limiting current (compliance voltage) are provided in Fig. 4. Note that the positive compliance voltages have their sign switched to more easily compare against the negative map, and the colormap limits used are different (plotting to the same limits makes the negative map almost flat). The negative bias compliance map in Fig. 4(a) clearly shows visible spatially correlated features of high and low conductivity, with a feature size of 30-50 nm (lower conductivity implies a higher bias magnitude is needed to achieve the limiting current). A significant variation in cutoff voltages exists for the anodic process (Fig. 4(b)) compared to the cathodic process where features appear spatially correlated but feature size is much smaller (10-20 nm). Furthermore, the statistical distribution of the anodic biases is significantly larger (the mean and standard deviation for cathodic biases are $-13 \pm 2$ V and for anodic are $11 \pm 3$ V). Few of the features in the compliance map can be correlated with surface morphology for the negative voltage map and almost none for the positive voltage map, suggesting that they originate from internal defects not topographic cross talk. Certain features can also be observed in both polarities as having particularly high or low voltages to reach the compliance current suggesting the two processes probed are not entirely independent.

To obtain the mechanistic insight into this data, we consider the conduction process in MIECs following the theory developed by Riess and others.[14,15,23,24] We note that while classical I-V

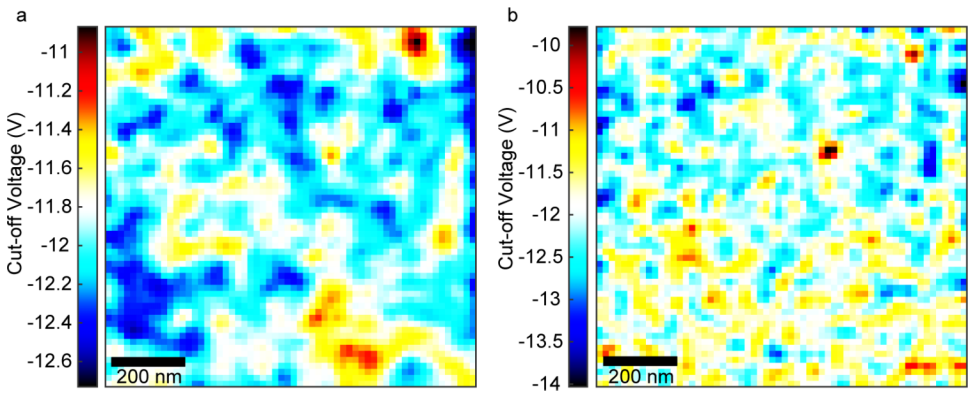


FIG. 4. (a) Negative compliance voltage map (smoothed with a Gaussian filter) on 1 $\mu$m square of the ceria film with a compliance limit of 100 pA. (b) Positive compliance voltage map (sign inverted) for the same area (and the same filter) with a compliance limit of 100 pA.

analyses for mixed electronic-ionic conductors were developed for the uniform field case, their predictions are expected to be qualitatively correct in the case of a localized probe. Furthermore, in certain cases, the transport equations derived for a uniform field can be used directly, with the probe-surface contact radius becoming the relevant length scale and substituting, for example, for sample thickness.

On the qualitative level, we note that the range of appropriate transport models can be defined based on the overall shape of the I-V curve and further verified against the known defect chemistry of the material and experimental condition (e.g., reversible vs. blocking electrodes). However, conductivity at the surfaces can be significantly different from bulk due to the nanoscale confinement effect,[25,26] surface space charge layers,[27] and possible additional conductive modalities, e.g., due to protons.[28] Furthermore, the nanoscale nature of the SPM tip-surface contact can significantly affect its electrochemical nature due to both the high concentration of electric fields (high over-potentials enabling gas-solid reactions even at low temperatures) and gas exposure (e.g., continuum platinum field is blocking, porous platinum and nanoscale tip-surface contact are not). Hence, bulk defect chemistry provides a useful guideline but is expected to be insufficient for *a priori* predictions of nanoscale behavior in a SPM based experiment.

Ceria has a high propensity for ionic and electronic conduction, notably recent studies by the Lubomirsky group demonstrate that defects and defect dipoles in ceria can be mobile in sufficiently high fields at room temperature.[29,30] Ionic conduction is strongly enhanced in pulsed-laser deposition grown films, which often have high oxygen non-stoichiometry. We expect nonstoichiometric ceria to be an n-type semiconductor in which oxygen deficiency leads to oxygen vacancies in the cubic fluorite lattice with electrons from the removed oxygen atom interacting with neighboring cerium cations.

In a dry atmosphere, the possible surface reactions are those of oxygen reduction reaction (ORR) and oxygen evolution reaction (OER), given in Kröger-Vink notation[31] as

$$2Ce_{ce}^{x} + O_{o}^{x} \rightarrow 2Ce_{ce}' + V_{\ddot{O}} + \frac{1}{2}O_2(g). \quad (1)$$

The top electrode (tip-surface contact) is expected to be electronically conductive (metallic behavior) and ionically blocking for small biases but may allow oxygen evolution from the surface as bias is increased, leading to a non-zero ionic current and introduction of further vacancies and charge carriers. The bottom electrode is electronically conductive (metallic) but is likely to be ionically blocking at room temperature. Under the assumption that the electron concentration follows a pattern $n_e = 2N$, where $n_e$ is the number of electrons and N is the number of vacancies, the current voltage behavior for the ceria film under study will then be expected to follow the Hebb-Wagner model.[32,33]

When applying a bias across a MIEC with two blocking electrodes, a certain degree of polarization in the distribution of mobile ionic species is to be expected. This situation is not a charge distribution, but a case where the concentration of these species in the sample shows some gradation under the applied field.[34] If the value of x for $CeO_{2-x}$ is not constant across the thickness of the film but can vary with applied bias, then oxygen ions, and subsequently oxygen vacancies and associated quasi-free electrons, will differ across the film. The effect of this distribution on the electronic current has been discussed previously[35] and is predicted to give rise to self-limiting tan h(a) type curves which do not match the data recorded during this experiment. The cause of this departure from expected behavior is likely due to the use of a localized probe to measure the current.

One issue that may arise due to use of a SPM tip as an electrode is related to the change in defect concentrations across the film under an applied bias, an effect consolidated by the thickness of the film and the strong electric fields associated with the size of the probe tip. Under a negative tip bias, the positively charged vacancies migrate towards the film-tip interface and away from the substrate, whilst vacancies move towards the film-substrate interface and away from the probe tip under positive tip bias. Investigations into electronic conductivity in $CeO_{2-x}$ with varying x values show that conductivity is related to the departure from stoichiometry[11] and an important point to note is that in addition to decreasing defect concentrations, increasing defect numbers can also reduce conductivity when increased past a certain threshold.[36] As noted by the authors, this issue could

arise for a number of reasons such as defect interactions, localized electrons repelling one another, and a lack of suitable hopping steps for the polaron ($Ce^{4+}$ ions are required). Therefore, regions of particularly high or particularly low defect concentrations are expected to be poor electronic conductors in a polaron-hopping regime.

Attention is also required concerning the effects of potential mechanical strains on the lattice due to defect interactions and possible electrostriction under such concentrated fields. Recent research has shown that significantly strained films can show markedly different behaviors in their conductivity and defect interactions than those with equilibrium lattice positions.[37,38] Predicted causes for this include the alteration of ionic radii with different Ce valence states and electrostatic repulsion from oxygen vacancies.[39,40] Whilst quantifying such contributions is difficult, the high probability of local strain effects during measurement should not be ignored as it may lead to further amplification or reduction of non-equilibrium defect areas.

The prediction is therefore that the resistivity of the film increases with increasing bias based on the two extremes in defect concentration near the electrodes which increase with increasing voltage (fields are expected to be much higher at the top electrode due to the probe dimensions). Changes in the conductivity would result in the I-V measurements failing to follow the standard MIEC formulae potentially causing the lack of observed current until significant bias is applied. At higher bias, the I-V curves for a positive tip bias show a much steeper exponential increase than for negative tip bias potentially due to the initiation of oxygen evolution from the surface and the potential for electroforming mentioned earlier. Partial decomposition at a level below the accuracy of the topographic images may also explain some of the discrepancy in the cutoff mapping; further investigation of the scanned area with transmission electron microscopy would be needed to detect any oxygen evolution. It is also worth mentioning that many theories for electroforming within metal oxides predict an alignment of vacancies between the electrodes creating a thin filament path which exhibits partially metallic behavior or similar behavior near the interface due to charge carrier migration.[6] Therefore, regions rich or poor in charge carriers and/or defects can be expected to display highly complex behavior, and quantitative fits to data are difficult due to the unknown alteration in resistance on oxide concentration $(2 - x)$ and the strong possibility of defect interactions, mixed ionization defects, path disruptions to polaron hopping, differing electrode geometry, and the potential formation of metallic regions.[6]

To explain the difference in spatial variability (correlation length, feature size, and dispersion) for the cathodic and anodic conduction, one option to consider is the ionic dynamics of MIECs in the tip field. For negative bias, a high concentration of oxygen vacancies is expected at the tip-surface contact and a low concentration near the bottom electrode. The highest resistance region is expected to occur near the tip (assuming the region closer to pure $CeO_2$ provides the highest resistance) affecting an area with similar geometry, probing defect structure, and vacancy mobility close to the surface. For positive bias, the larger contribution to resistance is expected near the bottom electrode resulting in a greater diffusivity of conductivity due to the lack of a localized contact and therefore a reduced lack of correlation with surface features. Although some features in the compliance maps do relate to surface features, many regions do exist in which conductance does not follow topographic features suggesting differences in defect structure/mobility are being probed. For positive bias, no such correlation is easily visible in the topographic and conductance data, and probing the bottom electrode interface is predicted to be much more difficult using this technique, which may be further compounded by any unnoticed decomposition. These data, whilst unclear in their exact mechanism, provide information about the spatial inhomogeneity of conductance and allow us to investigate the top and bottom interfaces in the ceria film.

To summarize, a method for probing the defect structure of a mixed ionic electronic oxide film has been introduced. We utilize the vacancy dynamics under opposite polarities combined with geometrical size difference between the tip and the bottom electrode to spatially resolve the defect structure. This provides insight into the variation of conductance and suggests the existence of large spatial inhomogeneity that in standard electrochemical characterization methods will give rise to the resistive elements and affect the overall conductivity of the films on the macroscale.

We further note that the important role of electrochemical activity in voltage controlled SPM experiments is well-known since the early days of SPM.[41–44] It was shown recently that the

extent of stray electrochemical reactions is largely controlled by the total current that controls any over-potential in the tip-surface junction, rather than potential *per se*.[45] The proposed galvanostatic current-voltage measurements method, while trivial, can be beneficially used for probing tip-controlled electrochemistry in a spatially resolved fashion and also the exploration of physical systems such as conductance of ferroelectric domain wall conductance and tunneling barriers.

Finally, we note that this approach can be used to study local conductance behavior in other MIECs, including those for memristive and electroresistive applications, to elucidate the nanoscale factors controlling ionic and electronic transport. Furthermore, combination with STEM/TEM in the future will allow the elucidation of the microstructural and atomistic origins of the observed effects, directly linking functionality to local structure.

Part of this research was conducted at the Center for Nanophase Materials Sciences, which is sponsored at Oak Ridge National Laboratory by the Scientific User Facilities Division, U.S. Department of Energy. A.K. acknowledges support from the Royal Society (No. RG130604). This work was also supported by the Engineering and Physical Sciences Research Council [grant number EP/K502911/1 and EP/M506400/1].

[1] A. Kolmakov and M. Moskovits, Annu. Rev. Mater. Res. **34**, 151 (2004).
[2] N. Izu, W. Shin, I. Matsubara, and N. Murayama, Electrochemistry **73**, 478 (2005).
[3] N. Izu, W. Shin, N. Murayarna, and S. Kanzaki, Sens. Actuators, B **87**, 95 (2002).
[4] C. Ispas, J. Njagi, M. Cates, and S. Andreescu, J. Electrochem. Soc. **155**, F169 (2008).
[5] R. Waser, R. Dittmann, G. Staikov, and K. Szot, Adv. Mater. **21**, 2632 (2009).
[6] A. Sawa, Mater. Today **11**(6), 28 (2008).
[7] E. P. Murray, T. Tsai, and S. A. Barnett, Nature **400**, 649 (1999).
[8] A. Trovarelli, Catal. Rev. **38**, 439 (1996).
[9] B. Zhu, I. Albinsson, C. Andersson, K. Borsand, M. Nilsson, and B. E. Mellander, Electrochem. Commun. **8**, 495 (2006).
[10] H. L. Tuller and A. S. Nowick, J. Electrochem. Soc. **126**, 209 (1979).
[11] T. Suzuki, I. Kosacki, H. U. Anderson, and P. Colomban, J. Am. Ceram. Soc. **84**(9), 2007 (2001).
[12] H. L. Tuller and A. S. Nowick, J. Phys. Chem. Solids **38**, 859 (1977).
[13] E. B. Lavik, I. Kosacki, H. L. Tuller, Y. M. Chiang, and J. Y. Ying, J. Electroceram. **1**(1), 7 (1997).
[14] I. Riess and D. Cahen, J. Appl. Phys. **82**, 3147 (1997).
[15] I. Riess, Solid State Ionics **51**, 219 (1992).
[16] N. Yang, S. Doria, A. Kumar, J. H. Jang, T. M. Arruda, A. Tebano, S. Jesse, I. N. Ivanov, A. P. Baddorf, E. Strelcov, S. Licoccia, A. Y. Borisevich, G. Balestrino, and S. V. Kalinin, Nanotechnology **25**(7), 075701 (2014).
[17] P. Gao, Z. C. Kang, W. Y. Fu, W. L. Wang, X. D. Bai, and E. G. Wang, J. Am. Chem. Soc. **132**, 4197 (2010).
[18] M. Molinari, S. C. Parker, D. C. Sayle, and M. S. Islam, J. Phys. Chem. **116**, 7073 (2012).
[19] K. Szot, W. Speier, G. Bihlmayer, and R. Waser, Nat. Mater. **5**, 312 (2006).
[20] D. B. Strukov, G. S. Snider, D. R. Stewart, and R. S. Williams, Nature **453**, 80 (2008).
[21] D. S. Jeong, H. Schroeder, U. Breuer, and R. Waser, J. Appl. Phys. **104**, 123716 (2008).
[22] A. Kumar, T. M. Arruda, Y. Kim, I. N. Ivanov, S. Jesse, C. W. Bark, N. C. Bristowe, E. Artacho, P. B. Littlewood, C.-B. Eom, and S. V. Kalinin, ACS Nano **6**, 3841 (2012).
[23] I. Riess, J. Electroceram. **17**, 247 (2006).
[24] I. Riess, Solid State Ionics **7**, 475 (1992).
[25] A. Kossoy, Y. Feldman, E. Wachtel, K. Gartsman, I. Lubomirsky, J. Fleig, and J. Maier, Phys. Chem. Chem. Phys. **8**, 1111 (2006).
[26] J. Maier, Nat. Mater. **4**, 805 (2005).
[27] B. W. Sheldon and V. B. Shenoy, Phys. Rev. Lett. **106**, 216104 (2011).
[28] B. Zhu, I. Albinsson, and B. E. Mellander, Ionics **4**, 261 (1998).
[29] S. Swaroop, M. Kilo, A. E. Kossoy, I. Lubomirsky, and I. Riess, Solid State Ionics **179**, 1205 (2008).
[30] A. Kossoy, Y. Feldman, E. Wachtel, I. Lubomirsky, and J. Maier, Adv. Funct. Mater. **17**, 2393 (2007).
[31] F. A. Kröger and H. J. Vink, Solid State Phys. **3**, 307 (1956).
[32] M. H. Hebb, J. Chem. Phys. **20**, 185 (1952).
[33] H. Rickert and C. Wagner, Z. Elektrochem. **64**, 1112 (1960).
[34] I. Riess, Solid State Ionics **157**(1–4), 1 (2003).
[35] Z. Rosenstock and I. Riess, Solid State Ionics **136–137**, 921 (2000).
[36] I. K. Naik and T. Y. Tien, J. Phys. Chem. Solids **39**, 3 (1978).
[37] J. L. Rupp, E. Fabbri, D. Marrocchelli, J.-W. Han, D. Chen, E. Traversa, H. L. Tuller, and B. Yildiz, Adv. Funct. Mater. **24**, 1562 (2014).
[38] M. J. D. Rushton, A. Chroneos, S. J. Skinner, J. A. Kilner, and R. W. Grimes, Solid State Ionics **230**, 37 (2013).
[39] D. Marrocchelli, S. R. Bishop, H. L. Tuller, and B. Yildiz, Adv. Funct. Mater. **22**, 1958 (2012).
[40] J. L. M. Rupp, Solid State Ionics **207**, 1 (2012).
[41] J. Maier, *Physical Chemistry of Ionic Materials: Ions and Electrons in Solids* (Wiley, New York, 2004).
[42] T. Tsuruoka, K. Terabe, T. Hasegawa, and M. Aono, Nanotechnology **21**, 425205 (2010).
[43] S. V. Kalinin and D. A. Bonnell, Nano Lett. **4**, 555 (2004).
[44] F. R. F. Fan, A. J. Bard, R. Guckenberger, and M. Heim, Science **270**, 1849 (1995).
[45] S. V. Kalinin, S. Jesse, A. Tselev, A. P. Baddorf, and N. Balke, ACS Nano **5**, 5683 (2011).